ADVANCED FUNCTIONAL MATERIALS
www.afm-journal.de

Materials Views
www.MaterialsViews.com

Chirality of Metal Nanoparticles in Chiral Mesoporous Silica

*Junjie Xie, Yingying Duan, and Shunai Che**

Chiroptical properties of pure inorganic material have been achieved by dispersing small amounts of achiral Ag nanoparticles into highly ordered chiral mesoporous silica. There are three types of chirality in chiral mesoporous silica: i) the helical hexagonal surface, ii) the helical pore orientation, and iii) the helical arrangement of aminopropyl groups on the surface of the mesopores, all of which impart plasmonic circular dichroism and have been investigated by introducing Ag nanoparticles into the as-made, calcined and extracted chiral mesoporous silica, respectively. The three types of optical response originate from asymmetric plasmon-plasmon interactions of achiral Ag nanoparticles in three types of chiral environments. Among the three sources of chirality, the helical pore orientation was considered to be predominantly responsible for the optical response owing to the high efficiency of nanoscale chirality. Interestingly, large Ag nanoparticles aggregation as a result of calcination still resulted in a strong optical activity, even the chiral mesostructure was destroyed completely. Rather than the pitch length, the length of helical channel was more effective for increasing the intensity of plasmonic circular dichroism due to longitudinal propagation of Ag nanoparticles along helical channel. Such novel chiral inorganic material will bring new opportunities in non-linear optics, biosensors and chiral recognition.

1. Introduction

Chirality is expressed at various levels, from a single molecule to supramolecular systems, in different aspects of nature.[1] Chiral molecules and materials can be designed to perform elaborate functions. These molecules are used in a variety of systems, such as pharmaceuticals, catalysts, and optoelectronic devices, and have been rapidly evolving into a major research area in the field of biomedicine and material science.[1] The chiroptical properties of functional materials rely not only on the chirality of the building blocks but also on chiral assemblies of building blocks in chiral host materials. To date, metal noparticles (NPs) capped with chiral organic molecules and assembled in chiral environments exhibiting optically active absorption effects in the visible light spectrum have been extensively reported because of their novel physical and chemical properties of surface plasmon resonance (SPR).[2] Chiral metal NPs and their nanocomposites are considered to have great potential as nanoscale elements for constructing functional materials, such as catalysts, non-linear optics and biological sensors and dectectors.[3]

Since the first report of chiral gluvtathione-protected Au NPs exhibiting particular optical activity in SPR by Schaaff and Whetten,[4] diverse types of chirality in metal NPs have been shown to create plasmonic circular dichroism (PCD).[5] These systems include metal NPs capped with various small chiral molecules, or biological macromolecules such as DNA, peptides, and proteins.[6] Three possible explanations have been proposed to address the observed PCD signal of the above metal NPs: 1) the formation of a chiral core; 2) electronic interactions between chiral molecules and an achiral core; and 3) chiral arrangement of chiral molecules adsorbed on achiral core were extensively applied to explain the origination of chirality.[2a,b,4,7]

Additionally, achiral plasmonic metal (Au or Ag) NPs arranged with a chiral geometry were regarded as another source of PCD effects in the various supported scaffolds, such as DNA, peptides, polymers, organic fibers, cholesteric liquid crystals and nematic chiral mesoporous silica structures.[8] These chiral supporters provide an important chiral host for the organization of metal NPs in chiral arrangements for observed PCD signals, although the effect of a chiral environment on PCD signal creation is still not clear. Some theoretical calculations and simulations show that these PCD signals may result from Coulombic plasmonic interactions between non-chiral NPs arranged in a chiral manner, e.g., assembled in asymmetric tetrahedral frames or helically organized arrangements.[9] To better understand this mechanism, various aspects related to the creation of PCD signals still need to be developed and investigated.

Herein, we describe our efforts to determine the effect of three types chirality existed simultaneously in chiral mesoporous silica (CMS) on the creation of PCD signals. As shown in **Scheme 1**, we have recently achieved the synthesis of highly ordered CMS with chiral channels based on the self-assembly of chiral anionic surfactant N-acylamino acid using 3-aminopropyl-triethoxysilane (APES) as a co-structure-directing agent

Dr. J. Xie, Y. Duan, Prof. S. Che
School of Chemistry and Chemical Engineering
State Key Laboratory of Metal Matrix Composites
Shanghai Jiao Tong University
800 Dongchuan Road,
Shanghai, 200240, P. R. China
E-mail: chesa@sjtu.edu.cn

DOI: 10.1002/adfm.201200588

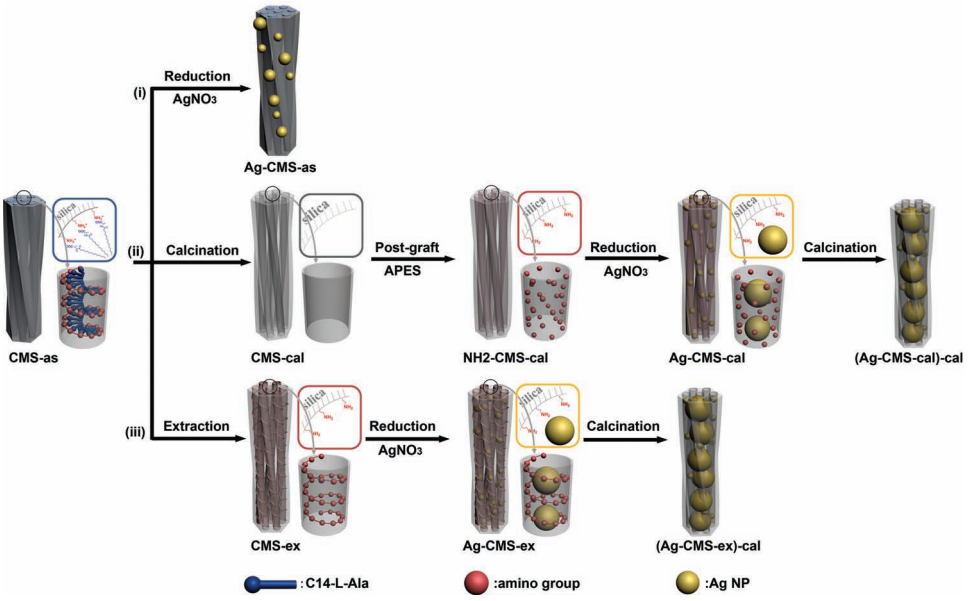

Scheme 1. Illustration of Ag NPs synthesized, as well as reduction and subsequent calcination. CMS-as: synthesized with electrostatic interaction between the head-group of chiral surfactants and the amino group of APES. (i) Ag-CMS-as: synthesized by the reduction of $AgNO_3$ onto the chiral surface of CMS-as. (ii) CMS-cal: calcined first; NH_2-CMS-cal: functionalized with an amino group by introducing APES; Ag-CMS-cal: synthesized by the subsequent reduction of $AgNO_3$ into the chiral pores of NH_2-CMS-cal; (Ag-CMS-cal)-cal: large Ag NPs aggregates were embedded into the purely inorganic CMS by calcination. (iii) CMS-ex: extracted first; Ag-CMS-ex: synthesized by subsequent reduction of $AgNO_3$ into the amino group helically arranged chiral pores of CMS-ex; (Ag-CMS-ex)-cal: large Ag NPs aggregates embedded into the purely inorganic CMS by further calcination.

(CSDA) and tetraethyl orthosilicate (TEOS) as a silica source.[10] The CMS has a twisted hexagonal rod-like morphology with a diameter of 100–200 nm as well as a pitch length of 0.5–1.5 μm. The helicity of CMS is readily tuned by changing stirring rate and the molar ratio of additional acid relative to surfactant.[11] As-synthesized CMS is denoted "CMS-as." After removing surfactant through calcination (CMS-cal), it has been confirmed that the hexagonal rod possesses hexagonally ordered chiral channels approximately 3.0 nm in diameter running along the rod axis while at the same time winding around the central axis of the rods with a different curvature.[12] Owing to the paired electrostatic interaction between the head group of the chiral anionic surfactant and the amino group of APES, helical arrays of amino groups were retained on the pore surface after extensive extraction (CMS-ex). It is clear that three types of chirality exist in CMS: (a) the helical hexagonal rod surface (CMS-as); (b) chiral channel orientation (CMS-cal); and (c) the helical arrangement of aminopropyl groups on the surface of the mesopores (CMS-ex).[13]

These three types of chirality-imparted chiral Ag NPs with various PCD signals were prepared by the reduction of silver nitrate using CMS-as, CMS-cal and CMS-ex as chiral scaffolds. (i) Ag NPs were deposited on the surface of the as-made CMS filled with the surfactants within the pores (Ag-CMS-as), which was used to express the first chirality of the CMS, i.e., the micrometer scale chiral surface-imparted PCD. (ii) To study the second type of chirality of CMS, i.e., the helical pore-imparted PCD, the as-made CMS was calcined and then functionalized with amino groups through a post treatment with APES (NH_2-CMS-cal). This resulted in a random arrangement of amino groups on the surface of the pores. The silver nitrate could then be easily introduced into the chiral pores due to coordination bonding between the Ag ion and the amino group. Subsequent reduction of $AgNO_3$ resulted in Ag NPs (Ag-CMS-cal). The PCD effect came from the Ag NPs both in the chiral pores and on the surface. (iii) The third type of chirality, i.e., the helical arrangement of aminopropyl groups on the surface of the CMS, was investigated using CMS-ex. Silver nitrate is easily bonded to the amino group helically oriented on the pore surface (Ag-CMS-ex). For these cases, the three types of chirality, i.e., chiral surface, chiral pores and chiral arranged amino groups, all of which would be able to endow the Ag NPs with chirality. Furthermore, the chirality of the large Ag NPs aggregated within the CMS by the subsequent calcination of Ag-CMS-cal and Ag-CMS-ex was also investigated. By calcination, the amino groups will be removed completely and the aggregates of NPs will destroy the mesoporous structure but would remain chiral porous fragments. These materials were denoted as (Ag-CMS-cal)-cal and (Ag-CMS-ex)-cal.

The left-handed CMS (L-CMS) and right-handed CMS (R-CMS) have been synthesized with N-miristoyl-L-alanine sodium salt (C14-L-AlaS) and N-miristoyl-D-alanine sodium salt (C14-D-AlaS) as templates, respectively. The chiral surface morphology, chiral pore structure and the presence of Ag NPs were confirmed with X-ray diffraction (XRD), scanning electron microscopy (SEM) and high-resolution transmission electron microscopy (HRTEM). The amino groups on the pore surface of CMS-cal and CMS-ex were all controlled using the same method and characterized using solid-state ^{13}C CP/MAS NMR spectra. The Ag/SiO2 molar ratios for all of the samples were determined using X-ray Fluorescence (XRF), which was

controlled in the same manner for both the Ag-CMS-cal and Ag-CMS-ex. Various PCDs were unambiguously detected using solid-state diffuse-reflectance circular dichroism (DRCD).[14]

2. Result and Discussion

2.1. Structure and DRCD of CMS-as, CMS-cal and CMS-ex

Figure 1A shows the XRD patterns of all three types of L- and R-CMSs, with three well-resolved peaks in the range 2θ = 1.5–6°, which were indexed as 10, 11 and 20 reflections, based on the two-dimensional hexagonal *p6mm* structure. These indices indicated that the mesoporous silica has a highly ordered hexagonal mesoscopic structure. After calcination, the unit cell parameter, a, decreased from approximately 5.5 to 5.0 nm (Table S1). Figure 1B shows the SEM and HRTEM images of antipodal extracted CMSs. The L-CMSs and R-CMSs particles both have well-defined twisted rod-like morphologies with a hexagonal cross-section.[45] The HRTEM images of the extracted samples show clear fringes, which are indicated with arrows. These fringes correspond to the interplanar spacing (10). After calcination, the original morphology and mesostructure of CMS were also preserved (not shown). As shown in solid-state ^{13}C CP/MAS NMR spectra (Figure 1C), the chiral templates were completely removed by extensive extraction with HCl-EtOH solution, and amino groups remained on the silica walls. Three resonance signals at 9.5, 21.7, and 42.6 ppm can be assigned to C1, C2, and C3 of the aminopropyl group, respectively. The concentration of the organic NH_2 groups was measured to be approximately 1.93 mmol/g. The calcined and extracted L-CMSs and R-CMSs showed very similar typical reversible type IV N_2 adsorption-desorption isotherms, confirming the existence of a uniform mesopore size distribution. Using the BJH (Barrett–Joyner–Halenda) method, pore diameters of 3.2 and 3.4 nm, respectively, were tabulated (Table S1, Figure S1 and Figure S2).

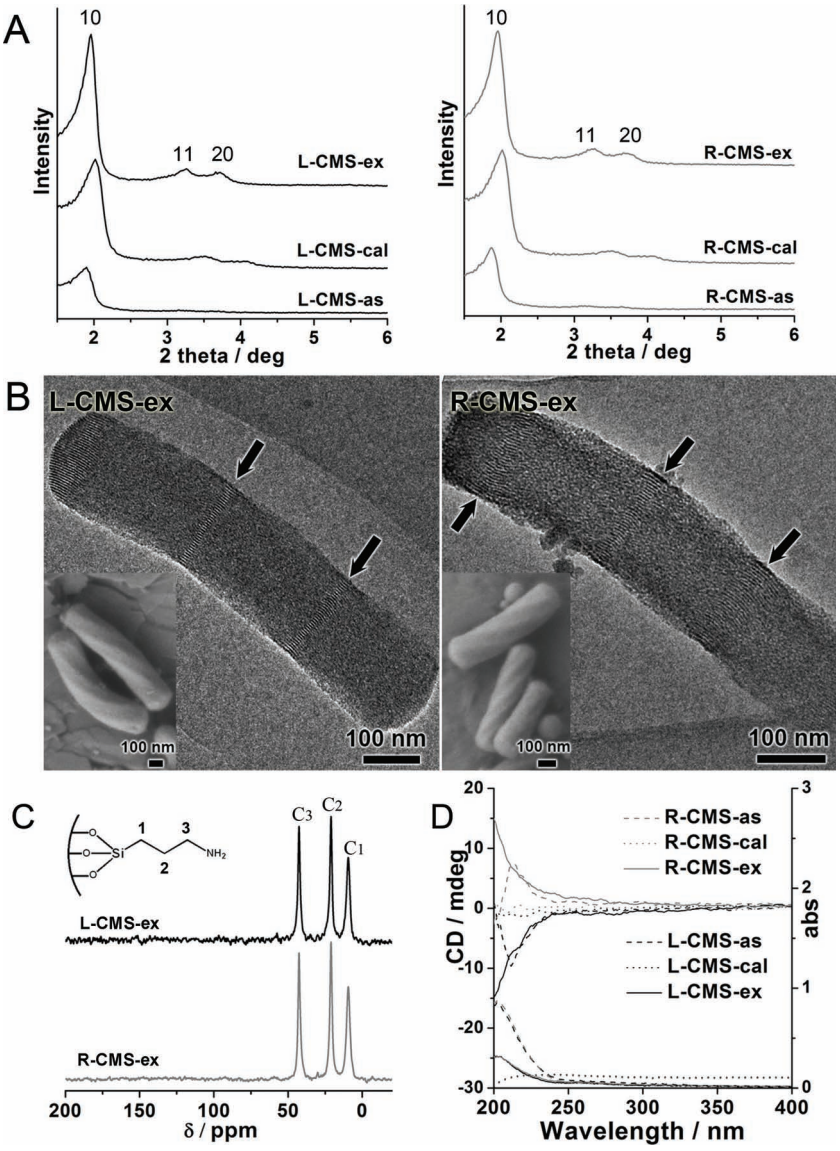

Figure 1. XRD patterns (A), HRTEM and SEM (inset) images (B), solid-state ^{13}C CP/MAS NMR spectra (C) and DRCD spectra (D) of L-(black lines) and R-(grey lines) CMS-as, CMS-cal and CMS-ex.

From Figure 1D, it can be observed that the antipodal L-CMS-as and the R-CMS-as exhibit a mirror-image DRCD spectra at 215 nm which is ascribed to the helical arrays of C14-L-(D)-AlaS in CMS-as. The CMS-cals show no CD signals, indicating that no chiral organics or helical arrangements remained in the calcined CMS and that the inorganic chiral morphology and pore structure does not produce a CD signal. The L-CMS-ex and R-CMS-ex revealed a strong negative and positive Cotton effect in the region below 250 nm, which may be due to the helical arrangement of amino groups on the surface of silica frameworks.[13,15]

2.2. Chiral rod Surface-Imparted PCD of Ag-CMS-as

From the TEM images of Ag-CMS-as, shown in **Figure 2**A, it was observed that the Ag NPs were randomly formed on the CMS rod. Ag particles between 3–10 nm, mostly larger than the mesopore size of 3.2 nm, were clearly observed, indicating that Ag NPs can seldom form in the actual mesopores of CMS-as. The small-angle XRD patterns of Ag-CMS-as exhibit one diffraction peak in the low-angle region, indicating that the ordered mesostructures have been retained. Figure S3 shows the wide-angle XRD pattern with four diffraction peaks

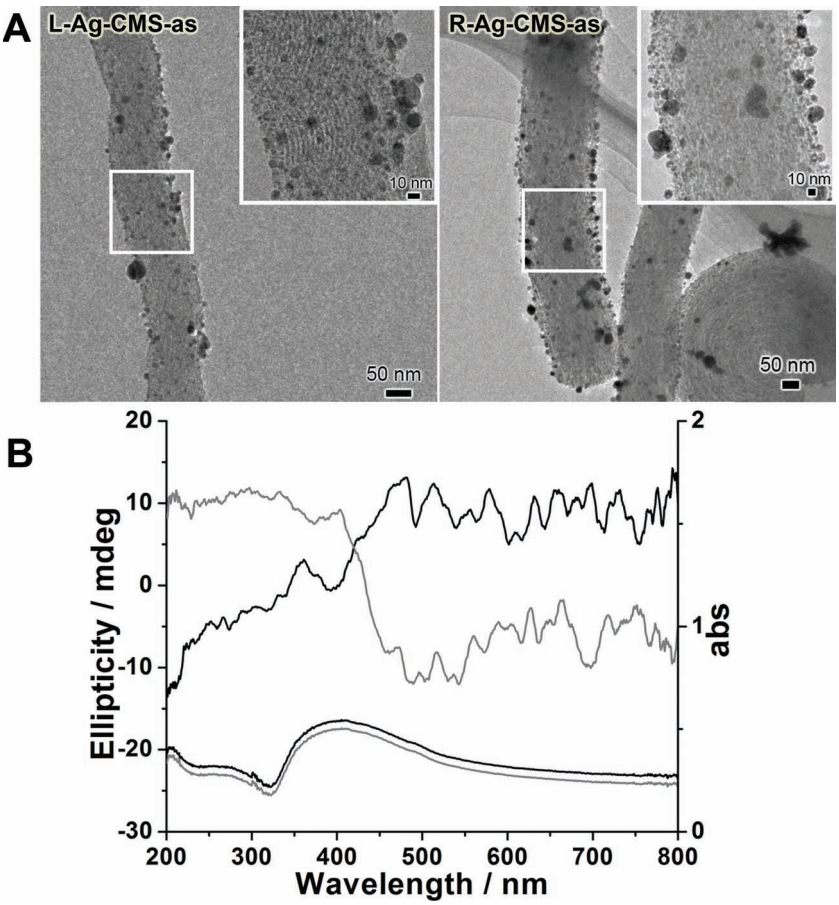

Figure 2. HRTEM images (A), DRCD and DRUV/Vis spectra (B) of L-(black lines) and R-(grey lines) -Ag-CMS-as.

discerned at $2\theta = 38.1$, 44.3, 64.5, and 77.5°, which are assigned to the (111), (200), (220), and (311) reflections of a face-centered cubic silver lattice.[3e,16] The Ag/SiO_2 molar ratios in both samples were measured to be approximately 0.01, which is smaller than those of CMS-cals and CMS-exs (vide post), indicating that $AgNO_3$ has difficulty incorporating into the surfactant layer of the CMS-as.

Figure 2B shows the DRCD and DRUV/Vis spectra of L-Ag-CMS-as and R-Ag-CMS-as. The DRUV/Vis spectra of the samples show a broad plasmon peak at approximately 405 nm, which is characteristic of silver nanoparticles.[16,17] DRCD spectra of L-Ag-CMS-as and R-Ag-CMS-as exhibit a weak positive and negative mirror-image response in the SPR region of the Ag NPs. The Ag NPs were asymmetrically assembled on the chiral surface through reduction of AgNO3. This arrangement was similar to that of Au NPs, which can asymmetrically organized themselves onto the chiral surface of peptide nanotubes or chiral organic fibers for surface plasmon coupled circular dichroism.[8g–8i] The weak DRCD intensity could be attributed to the large micro scale helical surface and lower ratio of helical surface to the total SiO_2, producing a weak chiral environment. To verify the effect of chiral surfactant assemblies on the PCD signals, Ag NPs doped with the C14-L-(D)-AlaS lipid assemblies were investigated. DRCD spectra of the mixture exhibit a symmetric peak at 215 nm, corresponding to helical assemblies of C14-L-(D)-AlaS. No CD signals were observed in the plasmon resonance region of Ag NPs (Figure S4), ruling out coupling between Ag NPs and chiral surfactant assemblies in Ag-CMS-as.

2.2. Chiral Pore-Imparted PCD for Ag-CMS-cal

To create extracted samples with similar coordination bonding interactions between Ag ions and amino groups for effective Ag NP introduction into pores, functional amino groups were incorporated into the mesopore surface through a post-graft treatment. The ^{13}C NMR spectrum of NH_2-CMS-cal (Figure S5) shows three resonance peaks at 8.5, 21.6, and 42.6 ppm; these are assigned to carbons C1, C2, and C3 of the aminopropyl group. XRD patterns of the NH_2-CMS-cal sample show a sharp diffraction peak at 2.05°, which is consistent with CMS-cal and indicates that a well-ordered mesoporous structure could be preserved after functionalization. The amount of amino groups on the CMS-cal surface, approximately 1.97 mmol/g, was confirmed qualitatively using elemental analysis. This value was the same to that of CMS-ex. Both L- and R-NH_2-CMS-cal show type IV N_2 adsorption isotherms that are similar to those of CMS-cal; however, the BJH pore size decreased from 3.2 to 2.8 nm due to tethering of the aminopropyl silane groups on the pore surface (Figure S6 and Table S1).

Figure 3A shows the HRTEM images of Ag-CMS-cal prepared through reduction of $AgNO_3$ in NH_2-CMS-cals. It can be observed that the helical pore structure was retained and that the Ag NPs were dispersed in the mesopores of NH_2-CMS-cal. Although there are also some large Ag NPs attached to outside of the CMS, Ag NPs with sizes smaller than the 3.2 nm pore size of CMS-cal were clearly observed within the twisted mesoporous channels using HRTEM. Small-angle XRD patterns show that the samples of NH_2-CMS-cal after loading with Ag NPs still retained an ordered mesostructure (Figure S7). This mesostructure was also confirmed with TEM images, as shown in Figure 3A. The wide-angle XRD pattern also shows four diffraction peak reflections of the face-centered cubic silver lattice. The broadness of these peaks suggests that the Ag NPs are small. The Ag/SiO_2 molar ratios of both the L- and R-Ag-CMS-cal were measured to be approximately 0.022. This molar ratio was larger than that of the Ag-CMS-as, indicating that a large amount of Ag was introduced into the pore. N_2 adsorption-desorption isotherms for L- and R-Ag-CMS-cal also showed similar types of IV curves with an average pore diameter of approximately 2.8 nm, similar to the samples before Ag loading. BET calculations indicated that the samples had 217 and 224 m^2/g of surface are and pore volumes of 0.18 and 0.20 cm^3/g, respectively (Figure S8). It can be calculated that only 1% of the pore

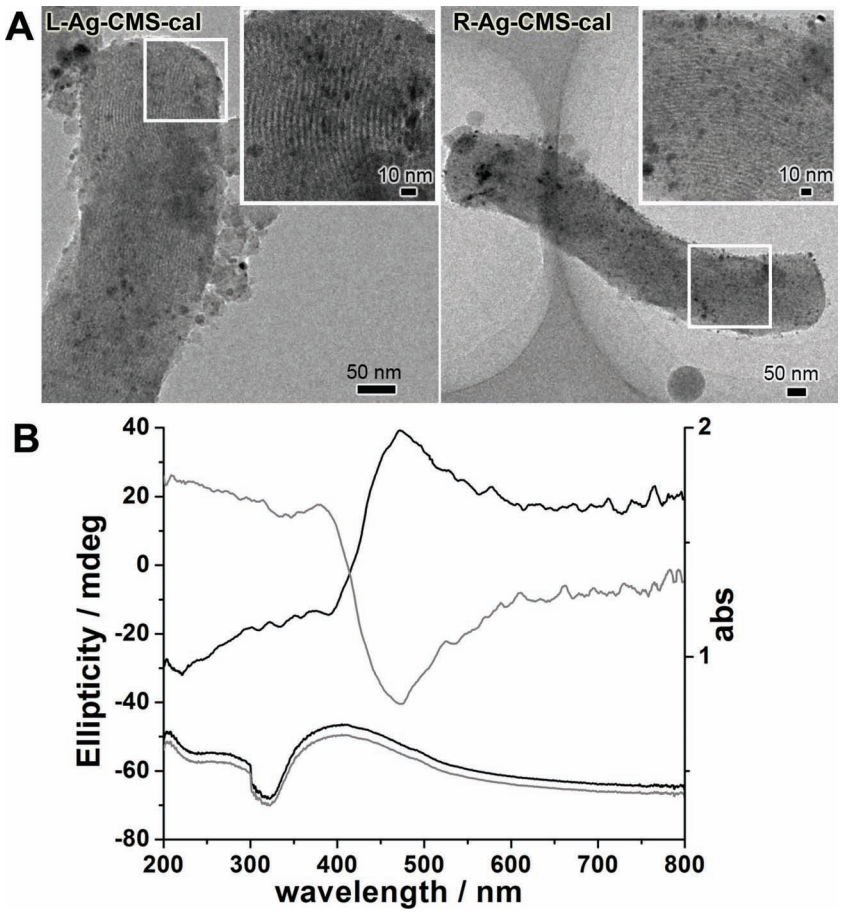

Figure 3. HRTEM images (A), DRCD and DRUV/Vis spectra (B) of L-(black lines) and R-(grey lines) -Ag-CMS-cal.

volume was occupied with the Ag NPs in the CMS-cal samples, confirming highly dispersed Ag NPs in the CMS materials, as shown in HRTEM images. The effect of different amount of Ag NPs loadings into the CMS on PCD response has been discussed in detail below.

From the UV/Vis spectra of Ag-CMS-cal shown in Figure 3B, a broad absorption band near 410 nm can be assigned to the surface plasmon frequency of Ag NPs.[3e,16] DRCD measurements of both L- and R-Ag-CMS-cal exhibit a large bisignate at 390 and 470 nm, respectively, with a crossover at 420 nm. The antipodal L- and R-Ag-CMS-cal complexes show strong mirror-imaged CD signals at approximately 45 millidegrees (mdeg). The L-Ag-CMS-cal sample exhibited a positive cotton effect followed by a negative one (positive couplet), and vice versa. As mentioned in the introduction, the chirality of the Ag NPs of these samples would arise from the chirality of the helical surface and helical pores. Undoubtedly, the observed PCD signals of the Ag NPs induced from the helical pores is the predominant factor in the Ag-CMS-cal. These signals are caused by the asymmetric plasmon-plasmon coupling interactions between Ag NPs in restricted nanometer sized chiral pores.[8k,9b]

Two possible factors may be responsible for the PCD sig-nals of these chiral Ag-CMS-cal complexes: (i) the chirality of the individual Ag NPs induced by the chiral pores of CMS-cal; or (ii) the plasmon-coulomb interaction between non-chiral Ag NPs arranged and positioned in porous chiral environments. To prove the intrinsic chirality of the individual Ag NPs in the CMS-cal samples, an aqueous solution of free Ag NPs was obtained by removing silica with NaOH or HF. No related CD signals were observed, which indicates that there was no optical activity associated with the individual Ag NPs in the Ag-CMS-cal (Figure S9). Therefore, the achiral Ag NPs should only produce an asymmetric plasmon interaction when in a chiral pore. The PCD signals of the Ag-CMS-cal are probably a result of the chiral environment induced collective response of the Ag NP plasmonic coupling.[2c,d,9a]

2.3. Helical Arrangement of Aminopropyl Groups Imparted PCD of Ag-CMS-ex

Helical arrangement of amino groups on the mesopore surface of the extracted CMS has been confirmed using probe molecule and chiroptical spectroscopy, as previously shown.[13] Ag NPs can also be easily introduced into the mesopores of CMS-ex by the reduction of Ag NO_3. Similar to Ag-CMS-cal, small Ag particles in chiral mesoporous channels and some large Ag NPs on the outer walls can be clearly observed from the TEM images of Ag-CMS-ex, as shown in **Figure 4**A. Small-angle XRD patterns show that both the Ag-L-CMS-ex and Ag-R-CMS-ex exhibit three well-resolved peaks of the 2D hexagonal mesostructure, indicating that well-ordered mesoporous structures have been preserved after the loading Ag NPs. The wide-angle XRD patterns also show four diffraction peaks of the face-centered cubic silver lattice. The broadness of these peaks reflects the small size of the Ag NPs (Figure S10). The Ag/SiO_2 molar ratios of both the L- and R-Ag-CMS-ex were measured to be approximately 0.023, which is the same as that of Ag-CMS-cal. The pore diameter is 3.4 nm, the same as the samples before Ag NP loading. The BET surface area and pore volume of the Ag-CMS-exs were 186 m^2/g and 0.28 cm^3/g, respectively, suggesting that only a small pore volume was occupied by the Ag NPs (Figure S11).

Figure 4B shows the DRCD and DRUV/vis spectra of Ag-CMS-ex. The UV/Vis spectra of the Ag-CMS-ex sample revealed a broad plasmonic absorption centered at approximately 420 nm, which is a slight bathochromic shift relative to the sample of Ag-CMS-cal.[3e] The DRCD measurements of the antipodal L-Ag-CMS-ex and R-Ag-CMS-ex complex show mirror-image CD spectra and exhibit two split peaks at 390 nm and 465 nm, respectively, with a crossover at 415 nm. Compared with Ag-CMS-cal, the intensity and shape of the Ag-CMS-ex PCD signals are almost unchanged. As mentioned in the introduction, the PCD of Ag-CMS-ex comes from the three types chirality of the CMS, i.e., the helical rod surface, helical pores

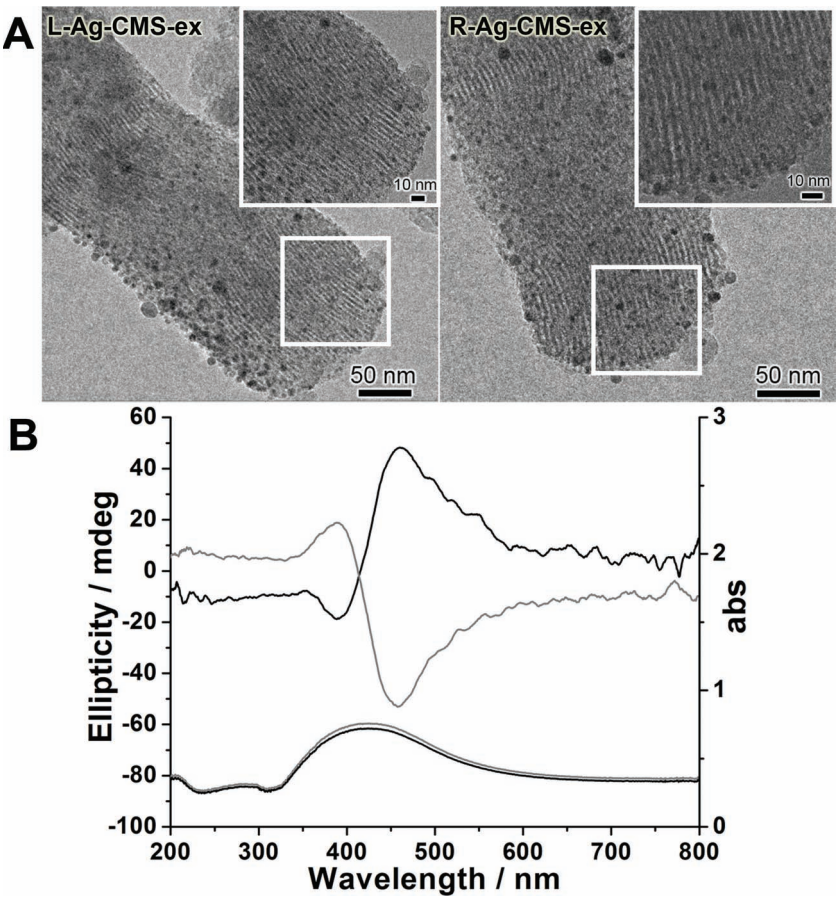

Figure 4. HRTEM images (A), DRCD and DRUV/Vis spectra (B) of L-(black lines) and R-(grey lines) -Ag-CMS-ex.

and helical arrangement of aminopropyl groups. Based on the two sets of DRCD spectra for Ag-CMS-cal and Ag-CMS-ex, and considering that the molar ratio of the Ag/SiO_2 for Ag-CMS-cal and Ag-CMS-ex are nearly identical, it seemed that the helical arrangement of amino groups immobilized on the mesopore surface in CMS-ex did not play a decisive role in imparting chirality to the Ag NPs. By contrast, among the three types chirality, porous chirality plays a dominant effect in inducing PCD. No CD signals have been observed from the Ag NPs released from sample of Ag-CMS-ex.

2.4. PCD of (Ag-CMS-cal)-cal and (Ag-CMS-ex)-cal

To further study the effect of the chiral pores of the CMS on the PCD of the Ag NPs. The functional amino groups which remained on the mesopores of both Ag-CMS-cal and Ag-CMS-ex were removed by calcination at 500 °C under argon flow (Figure S12). The uniformly sized Ag NPs, approximately 10 nm, which were embedded in the CMS-ex, were observed in HRTEM images shown in **Figure 5**A. The intensity of the (Ag-CMS-ex)-cal, which is shown as a wide-angle XRD pattern greatly increased after calcination, implying that the particle size of Ag NPs was larger than those in Ag-CMS-ex (Figure S13). The HRTEM images revealed that the interval of the intermittent fringes along the length of the CMS rod disappeared, indicating that there was a decrease in the mesoscopic ordering of the CMS. This decrease is in agreement with the small-angle XRD patterns in Figure S13. During calcination, the Ag NPs in chiral pores agglomerate into particles that are larger than the pore size of CMS-ex. These particles then rupture out of the mesopores in the CMS, leading to the deterioration of the mesostructure. The small BET surface area (76.6 m^2/g) and pore volume (0.104 cm^3/g) of the (Ag-CMS-ex)-cal also suggest the collapse of the mesostructure (Figure S14). However, the pore size distribution implies that chiral fragments still exist in these samples.[8f]

Interestingly, the UV/vis spectra of the Ag-L-CMS-ex and Ag-R-CMS-ex after calcination have an absorption peak at approximately 405 nm, which was ascribed to plasmon resonance.[3e] The DRCD spectra shows the typical peak-dip shape at 385 nm and 450 nm (Figure 5B). The shape of DRCD spectra is similar to that of Ag-CMS-ex, but the intensity of the DRCD signal decreased to 25 mdeg. Although the mesostructure of the sample deteriorated and the Ag NPs agglomerated into large size particles, the Ag-CMS-ex sample still possessed a strong optical response in the region of SPR. It is thought that the chiral porous fragments that remained would endow the Ag NPs with chirality. The disordered channel structure and large particle size would probably decrease the coupling of Ag NPs plasmon oscillations. The results from the (Ag-CMS-cal)-cal were similar to those from the sample of (ACMS-ex)-cal (Figure S15, S16 and S17).

2.5. The Effect of the Amount of Ag NPs Loaded into CMS on PCD

It has been proposed that the SPR and PCD of metal NPs is sensitive to the size and ordering of the NPs themselves, e.g., helix pitch and radius, the number of particles in a helix, and the geometry of the metal NPs.[3d,e,8g,9a,17] As previous experiments and simulations have shown, the number of particles greatly influences the shape and intensity of the PCD spectrum. Based on the reduction of $AgNO_3$ described above, the different amounts of Ag NPs were loaded into the CMS-ex repeatedly for different loading times. The samples were denoted as Ag-x-CMS-ex, where x is the time of the reduction treatment. XRF analysis showed that the molar ratios of the Ag/SiO_3 in the CMS-ex were 0.020, 0.065, 0.103 and 0.151 which corre-spond to the Ag-1-CMS-ex, Ag-2-CMS-ex, Ag-3-CMS-ex and Ag-4-CMS-ex, respectively. From the PCD results in **Figure 6**, although the bisignate shape of PCD spectrum was almost unchanged,

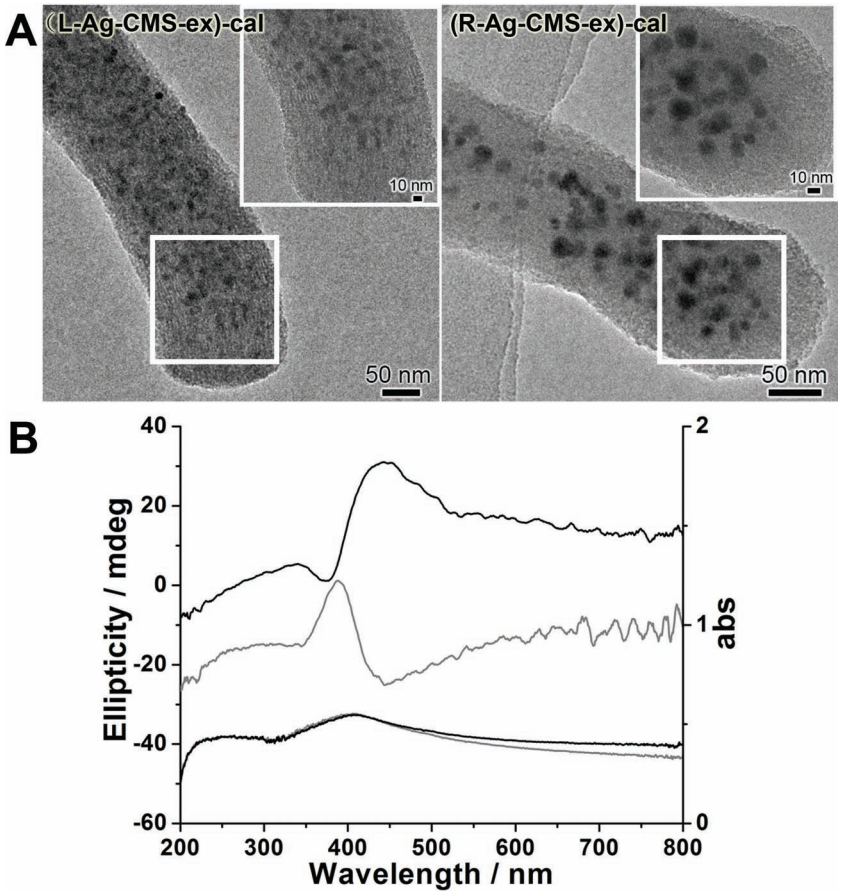

Figure 5. HRTEM images (A), DRCD and DRUV/Vis spectra (B) of L-(black lines) and R-(grey lines) -(Ag-CMS-ex)-cal.

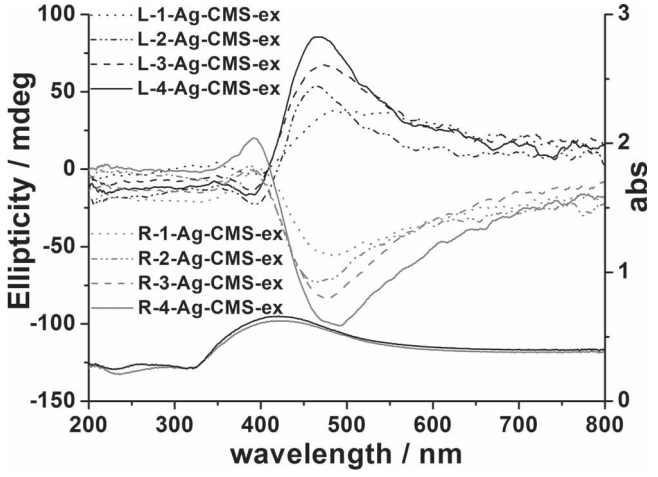

Figure 6. DRCD and DRUV/vis spectra of Ag NPs with different loading amounts in the CMS-ex.

the intensity of PCD signal progressively increased with the increasing amount of Ag NPs in the CMS-ex. The enhancement of the PCD response with the increased amount of Ag NPs was in accordance with the PCD signals within the dipolar theory of plasmon-plasmon interaction.[8g,9a,c,e] The robustness of the PCD response decreased when the Ag nanoparticles were introduced over the five loading times, despite the increase in the amount of Ag NPs due to the meso-structural collapse of CMS-ex.

2.6. The Effect of Different Pitch Length of CMS on PCD

As mentioned above, the helical pores of the CMS have a dominant effect on the chiral assemblies of Ag NPs and the observed PCD response. Helicity is the most important property of helical materials, therefore, CMSs with different pitch lengths have been employed to investigate the effect of helicity on the PCD response.[8g,9a,c]

The pitch length of the CMS was controlled by tuning the amount of acid in the synthetic procedure of the CMS. The Ag/SiO_2 molar ratio was set to approximately 0.020 (see Supporting information for experiment). **Figure 7** shows the SEM and TEM images of the samples with pitch lengths of 600, 900 and 1200 nm, denoted as CMS-ex-600, CMS-ex-900 and CMS-ex-1200, respectively (Figure S18). The average rod length was 400, 600 and 1200 nm similar to their pitch length. It is observed that rod length increased and diameter decreased, respectively, with increasing pitch length. DRCD spectra of the Ag-CMS-ex-600, Ag-CMS-ex-900 and Ag-CMS-ex-1200 show similar shaped PCD spectra, intensity increased with increasing pitch length shown in **Figure 8**. This phenomenon seems unusual because it is certain that a longer pitch length would lead to stronger chirality, due to Ag NPs propagating along longitudinal channel of CMS.[18] This finding well verified the calculated and simulated PCD results of Au NPs assembled in different helix pitch by Fan et al.[9a,c] On the other hand, while the pitch length was increased, the rod length was increased. Therefore, it can be considered that the rod length would have a dominant effect on PCD intensity in this CMS system, rather than pitch length and rod diameter. The longer CMS could accommodate a larger number of Ag NPs, which would then strengthen the PCD signal through more plasmon-plasmon coupling interactions. It is interesting to note that the transversal increasing number of Ag NPs is not effective for the PCD. Although there are theories related to such phenomena, it is still challenging to elucidate a clear mechanism for PCD signals chiral assemblies of metal NPs in our system. Further studies are under way to develop a detailed explanation for these discoveries.

3. Conclusions

In conclusion, we have successfully demonstrated three different types of chirality-imparted PCD signals for Ag NPs in

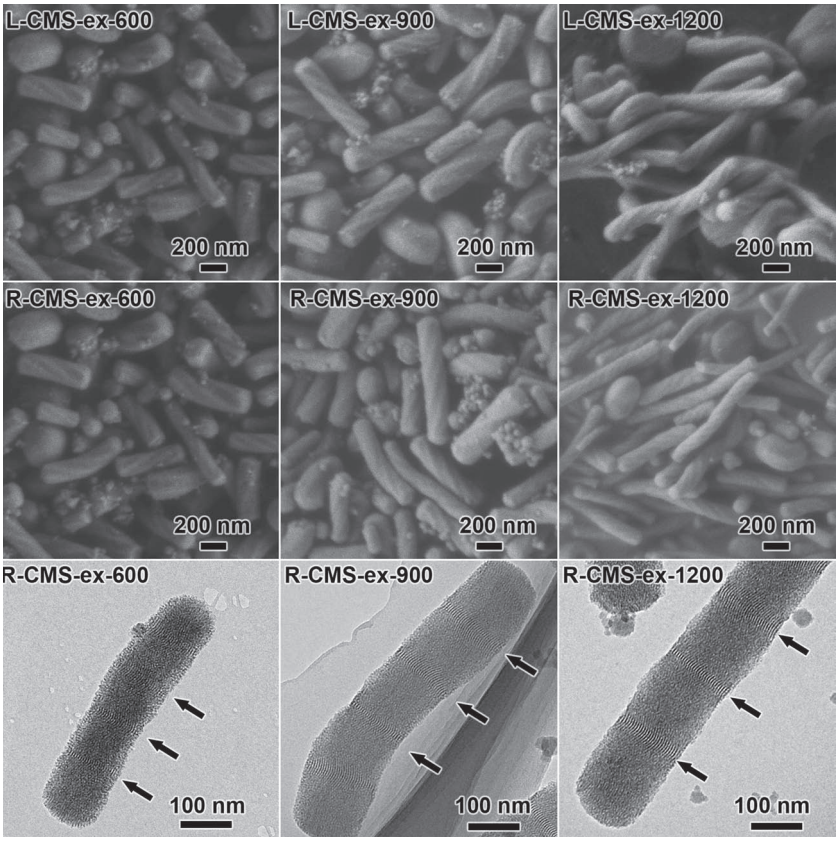

Figure 7. SEM and TEM images of L- and R-CMS-ex-600, CMS-ex-900, CMS-ex-1200. (The fringes indicated by the arrows correspond to the interplanar spacing of (10) planes, and the distance between two sets of fringes is one-sixth of one pitch length)

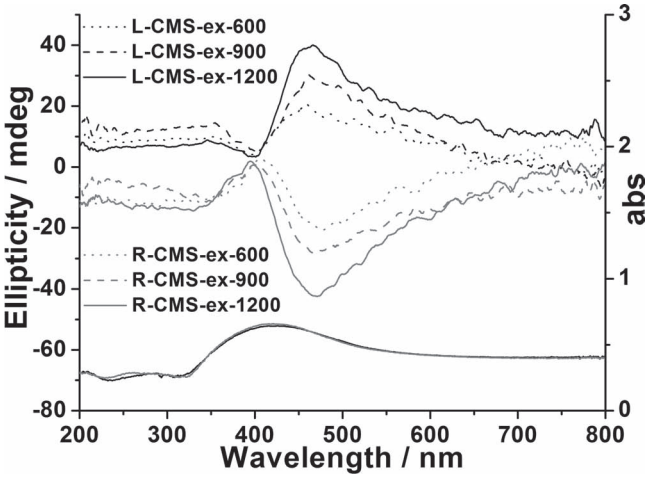

Figure 8. DRCD and DRUV/vis spectra of L- and R-Ag-CMS-ex-600, Ag-CMS-ex-900, Ag-CMS-ex-1200.

situ grown in CMS-as, CMS-cal, and CMS-ex. The distinct PCD response of the three types of samples showed plasmon-plasmon interactions with different chiral features of the CMS: i) twisted morphology, ii) chiral pore, and iii) helical arrangement of amino groups resting on mesopores. Among the three types of chirality, the chiral pore orientation was found to be the predominant factor for inducing a PCD response in the region of SPR owing to collectively asymmetric plasmon interactions of Ag NPs in the chiral pores. The length of helical channel was effective for increasing PCD intensity, rather than pitch length, due to Ag NPs longitudinal propagating along channel for the plasom-plasmon interaction. The assemblies of metal NPs in CMS will provide an ideal mode to create a better theoretical description of PCD signals based on calculations and simulations of plasmonic NPs in a 3D helical organization. Moreover, such chiral mesoporous material with the high efficiency of PCD response will develop new applications for biosensing, recognition and detection based on the importance of SPR in biological structures.[19]

4. Experimental Section

Chemicals: C14-L-AlaS, C14-D-Ala were synthesized according to previous reports.[51] Sodium hydroxide, hydrochloric acid, silver nitrate, and sodium borohydride were purchased from the Shanghai Chemical Company. TEOS was purchased from TCI and APES (98%) was from Azmax. All chemicals were used as received without further purification.

Synthesis of CMS-as, CMS-cal and CMS-ex: In a typical synthesis, C14-L-AlaS (0.32 g, 1 mmol) was dissolved in deionized water (30.0 g) while stirring at room temperature. Next, 0.2 mL of a 1.0 M HCl solution was added while vigorously stirring at room temperature to partially neutralize the salts. A mixture of TEOS (1.20 g, 6 mmol) and APES (0.22 g, 1 mmol) was then added to the reaction mixture while stirring at 20 °C. After 10 min of reaction time, the resultant material was left in a static condition for 2 days followed by an aging treatment at 353 K for 1 day. The products were recovered by centrifugal separation and then freeze-dried to obtain CMS-as. The surfactants were removed using exhaustive solid–liquid extraction overnight with a 1 M HCl solution in ethanol. The obtained product was CMS-ex, and with further calcination at 550 °C, CMS-cal was obtained.[43] The CMS with different pitch length prepared with different HCl addition amount. The synthesis molar composition was C14-L-AlaS:HCl:APES:TEOS:H2O = 1:x:1:6:1667, where x = 0.18, 0.20 and 022.[43[

Synthesis of NH_2-CMS-cal: CMS-cal (100 mg) was suspended in 25 ml of toluene, stirred for a few minutes at room temperature, and then allowed to react under reflux for 2 hours with 70 mg of APES, which was slowly added to the mixture. The resultant white solid was collected by centrifugation, washed twice with ethanol, and then freeze dried. The load amount of organic NH_2 groups was measured using elemental analysis.

Synthesis of Ag-CMS-as, Ag-CMS-cal and Ag-CMS-ex: In a typical synthesis, 20 mg of CMS-ex powder was dispersed in 2 ml of an $AgNO_3$ (10 mg/ml) solution and then stirred for 30 min at room temperature. The solid was separated out with a centrifuge and then washed with acetone to remove non-bound Ag ions. After freeze-drying, the powder was dispersed in 2 ml of a freshly prepared $NaBH_4$ solution (8 mg/g) and then stirred for 15 min to reduce the Ag ions to neutral Ag so that Ag NPs can form in the mesopores. The obtained dark yellow powder was centrifuged and dried in air under vacuum. The synthesis molar

ratio for all Ag/SiO_2 was approximately 0.02. The different amounts of Ag NPs were loaded into the CMS-ex repeatedly for different times, in same Ag loading method described above.

Synthesis of (Ag-CMS-cal)-cal and (Ag-CMS-ex)-cal: Ag-CMS-cal and Ag-CMS-ex were calcined at 500 °C for 6 h with a heating rate of 1 °C min^{-1} under flowing argon to remove any functional groups.

Characterization: Powder XRD patterns were recorded on a Rigaku D/Max 2000 powder diffractometer equipped with a CuKα radiation source. SEM images of all of the samples were taken with a JEOL JSM-7401F microscope at 1.0 kV. HRTEM observations were performed with a JEOL JEM-2100 microscope operating at 200 kV. The N_2 adsorption–desorption isotherms were obtained at 77 K with a Quantachrome NOVA 4200E surface area & pore size analyzer. Solid-state ^{13}C CP/MAS NMR spectra were collected with an Oxford AS400 NMR spectrometer at 100 MHz and a sample spinning frequency of 3 kHz. CHN elemental analysis was performed with a Perkin-Elmer Model 2400-II analyzer. Quantitative evaluation of the metal ions in the mesoporous silica was conducted using a Shimadzu XRF 1800 Spectrometer. UV/Vis (UV) spectra and diffuse-reflectance (DRUV) spectra were taken with a Shimadzu UV-2450 spectropolarimeter fitted with a DRUV apparatus. DRCD spectra were taken using a JASCO J-815 spectropolarimeter fitted with DRCD apparatus. It should be noted that all the present DRCD sample spectra were obtained by averaging the signals at different angles by rotating the sample in order to disregard the effect of linear birefringence (LB) and linear dichroism (LD).

Supporting Information

Supporting Information is available from the Wiley Online Library or from the author.

Acknowledgements

This work was supported by the National Natural Science Foundation of China (Grant No. 20890121) and the 973 project (2009CB930403) of China. The authors thank Instrumental Analysis Center of Shanghai Jiaotong University for their collaboration on CD measurements.

Received: February 29, 2012
Revised: April 19, 2012
Published online: May 25, 2012

[1] a) I. Agranat, H. Caner, J. Caldwell, *Nat. Rev. Drug Discov.* **2002**, *1*, 753; b) T. E. Gier, X. Bu, P. Feng, G. D. Stucky, *Nature* **1998**, *395*, 154.

[2] a) C. Gautier, T. Burgi, *ChemPhysChem* **2009**, *10*, 483; b) C. Noguez, I. L. Garzon, *Chem. Soc. Rev.* **2009**, *38*, 757; c) A. O. Govorov, Y. K. Gun'ko, J. M. Slocik, V. A. Gérard, Z. Fan, R. R. Naik, *J. Mater. Chem.* **2011**, *21*, 16806; d) A. Guerrero-Martínez, J. L. Alonso-Gómez, B. Auguié, M. M. Cid, L. M. Liz-Marzán, *Nano Today* **2011**, *6*, 381; e) V. Kitaev, *J. Mater. Chem.* **2008**, *18*, 4745; f) Y. Xia, Y. Zhou, Z. Tang, *Nanoscale* **2011**, *3*, 1374; g) M. Yang, N. A. Kotov, *J. Mater. Chem.* **2011**, *21*, 6775.

[3] a) M.-C. Daniel, D. Astruc, *Chem. Rev.* **2003**, *104*, 293; b) M. Tamura, H. Fujihara, *J. Am. Chem. Soc.* **2003**, *125*, 15742; c) Z. Nie, A. Petukhova, E. Kumacheva, *Nat Nano* **2010**, *5*, 15; d) N. L. Rosi, C. A. Mirkin, *Chem. Rev.* **2005**, *105*, 1547; e) M. Rycenga, C. M. Cobley, J. Zeng, W. Li, C. H. Moran, Q. Zhang, D. Qin, Y. Xia, *Chem. Rev.* **2011**, *111*, 3669; f) Z. Li, Z. Zhu, W. Liu, Y. Zhou, B. Han, Y. Gao, Z. Tang, *J. Am. Chem. Soc.* **2012**, *134*, 3322; g) N. A. Kotov, *J. Mater. Chem.* **2011**, *21*, 16673.

[4] T. G. Schaaff, R. L. Whetten, *J. Phys. Chem. B* **2000**, *104*, 2630.

[5] C. Gautier, T. Bürgi, *J. Am. Chem. Soc.* **2008**, *130*, 7077.

[6] a) N. Nishida, H. Yao, T. Ueda, A. Sasaki, K. Kimura, *Chem. Mater.* **2007**, *19*, 2831; b) A. Sánchez-Castillo, C. Noguez, I. L. Garzón, *J. Am. Chem. Soc.* **2010**, *132*, 1504; c) Y. Zhou, Z. Zhu, W. Huang, W. Liu, S. Wu, X. Liu, Y. Gao, W. Zhang, Z. Tang, *Angew. Chem. Int. Ed.* **2011**, *50*, 11456; d) A. O. Govorov, *J. Phys. Chem. C* **2011**, *115*, 7914; e) H. Behar-Levy, O. Neumann, R. Naaman, D. Avnir, *Adv. Mater.* **2007**, *19*, 1207; f) G. Shemer, O. Krichevski, G. Markovich, T. Molotsky, I. Lubitz, A. B. Kotlyar, *J. Am. Chem. Soc.* **2006**, *128*, 11006; g) J. M. Slocik, A. O. Govorov, R. R. Naik, *Nano Lett.* **2011**, *11*, 701; h) I. Carmeli, I. Lieberman, L. Kraversky, Z. Fan, 4A. O. Govorov, G. Markovich, S. Richter, *Nano Lett.* **2010**, *10*, 2069; i) Z. Zhu, W. Liu, Z. Li, B. Han, Y. Zhou, Y. Gao, Z. Tang, *ACS Nano* **2012**, *6*, 2326.

[7] Y. Zhou, M. Yang, K. Sun, Z. Tang, N. A. Kotov, *J. Am. Chem. Soc.* **2010**, *132*, 6006.

[8] a) J. Sharma, R. Chhabra, A. Cheng, J. Brownell, Y. Liu, H. Yan, *Science* **2009**, *323*, 112; b) A. J. Mastroianni, S. A. Claridge, A. P. Alivisatos, *J. Am. Chem. Soc.* **2009**, *131*, 8455; c) C. L. Chen, P. Zhang, N. L. Rosi, *J. Am. Chem. Soc.* **2008**, *130*, 13555; d) G. D. Lilly, A. Agarwal, S. Srivastava, N. A. Kotov, *Small* **2011**, *7*, 2004; e) F. Leroux, M. Gysemans, S. Bals, K. J. Batenburg, J. Snauwaert, T. Verbiest, C. Van Haesendonck, G. Van Tendeloo, *Adv. Mater.* **2010**, *22*, 2193; f) H. S. Oh, S. Liu, H. Jee, A. Baev, M. T. Swihart, P. N. Prasad, *J. Am. Chem. Soc.* **2010**, *132*, 17346; g) A. Guerrero-Martínez, B. Auguié, J. L. Alonso-Gómez, Z. Džolić, S. Gómez-Graña, M. Žinić, M. M. Cid, L. M. Liz-Marzán, *Angew. Chem. Int. Ed.* **2011**, *50*, 5499; h) J. George, K. G. Thomas, *J. Am. Chem. Soc.* **2010**, *132*, 2502; i) Y. Li, M. Liu, *Chem. Commun.* **2008**, 5571; j) R.-Y. Wang, H. Wang, X. Wu, Y. Ji, P. Wang, Y. Qu, T.-S. Chung, *Soft Matter* **2011**, *7*, 8370; k) H. Qi, K. E. Shopsowitz, W. Y. Hamad, M. J. MacLachlan, *J. Am. Chem. Soc.* **2011**, *133*, 3728.

[9] a) Z. Fan, A. O. Govorov, *Nano Lett.* **2010**, *10*, 2580; b) W. Chen, A. Bian, A. Agarwal, L. Liu, H. Shen, L. Wang, C. Xu, N. A. Kotov, *Nano Lett.* **2009**, *9*, 2153; c) Z. Fan, A. O. Govorov, *J. Phys. Chem. C* **2011**, *115*, 13254; d) A. O. Govorov, Z. Fan, P. Hernandez, J. M. Slocik, R. R. Naik, *Nano Lett.* **2010**, *10*, 1374; e) B. Auguié, J. L. Alonso-Gómez, A. s. Guerrero-Martínez, L. M. Liz-Marzán, *J. Phys. Chem. Lett.* **2011**, *2*, 846.

[10] S. Che, Z. Liu, T. Ohsuna, K. Sakamoto, O. Terasaki, T. Tatsumi, *Nature* **2004**, *429*, 281.

[11] a) H. Jin, Z. Liu, T. Ohsuna, O. Terasaki, Y. Inoue, K. Sakamoto, T. Nakanishi, K. Ariga, S. Che, *Adv. Mater.* **2006**, *18*, 593; b) H. Jin, H. Qiu, Y. Sakamoto, P. Shu, O. Terasaki, S. Che, *Chem. Eur. J.* **2008**, *14*, 6413.

[12] T. Ohsuna, Z. Liu, S. Che, O. Terasaki, *Small* **2005**, *1*, 233.

[13] H. Qiu, Y. Inoue, S. Che, *Angew. Chem. Int. Ed.* **2009**, *48*, 3069.

[14] R. Kuroda, T. Harada, Y. Shindo, *Rev. Sci. Instrum.* **2001**, *72*, 3802.

[15] a) J. Xie, H. Qiu, S. Che, *Chem. Eur. J.* **2012**, *18*, 2559; b) H. Qiu, S. Che, *Chem. Soc. Rev.* **2011**, *40*, 1259.

[16] I. Lieberman, G. Shemer, T. Fried, E. M. Kosower, G. Markovich, *Angew. Chem. Int. Ed.* **2008**, *47*, 4855.

[17] N. J. Halas, S. Lal, W. S. Chang, S. Link, P. Nordlander, *Chem. Rev.* **2011**, *111*, 3913.

[18] W. H. Weber, G. W. Ford, *Phys. Rev. B* **2004**, *70*, 125429.

[19] a) G. V. Hartland, *Chem. Rev.* **2011**, *111*, 3858; b) M. R. Jones, K. D. Osberg, R. J. Macfarlane, M. R. Langille, C. A. Mirkin, *Chem. Rev.* **2011**, *111*, 3736.